Accepted Manuscript

Development of xanthene dyes containing arylacetylenes: The role of acetylene linker and substituents on the aryl group

Ryo Hirata, Ayame Torii, Kenichi Kawano, Shiroh Futaki, Ayumi Imayoshi, Kazunori Tsubaki

PII: S0040-4020(18)30538-6

DOI: 10.1016/j.tet.2018.05.019

Reference: TET 29526

To appear in: *Tetrahedron*

Received Date: 17 March 2018

Revised Date: 2 May 2018

Accepted Date: 7 May 2018

Please cite this article as: Hirata R, Torii A, Kawano K, Futaki S, Imayoshi A, Tsubaki K, Development of xanthene dyes containing arylacetylenes: The role of acetylene linker and substituents on the aryl group, *Tetrahedron* (2018), doi: 10.1016/j.tet.2018.05.019.

Development of xanthene dyes containing arylacetylenes:

- The role of acetylene linker and substituents on the aryl group -

Ryo Hirata,[a] Ayame Torii,[a] Kenichi Kawano,[b] Shiroh Futaki,[b] Ayumi Imayoshi,[a] Kazunori Tsubaki [a*]

a. Graduate School of Life and Environmental Sciences, Kyoto Prefectural University, Shimogamo, Sakyo-ku, Kyoto 606-8522, Japan.

b. Institute for Chemical Research, Kyoto University, Uji, Kyoto 611-0011, Japan.

Graphical Abstract

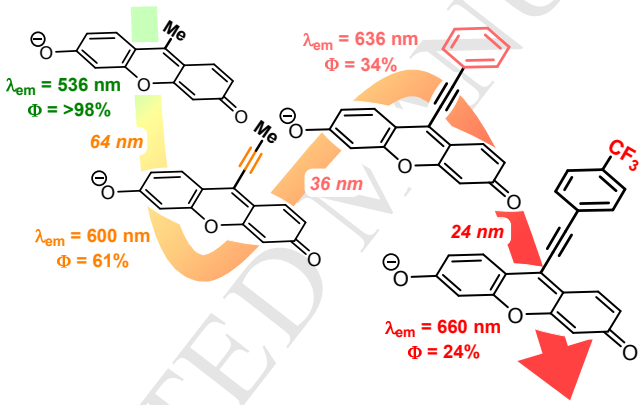

Keywords: xanthene dyes; fluorescein; phenylacetylene

Abstract

Fluorescent dyes possessing a variety of arylacetylenes at the 9-position of a xanthene skeleton were synthesized and their optical properties were investigated. The π system effectively expanded over the xanthene skeleton and the aryl group through the triple bond. Starting from the emission wavelength (λ_{em}) of 9-methyl xanthene **20** in basic DMSO solution at 536 nm, the emission wavelengths gradually shifted to the red region for methylacetylene **17** (λ_{em} = 600 nm), phenylacetylene **5** (λ_{em} = 636 nm), and *p*-CF_3-phenylacetylene **11** (λ_{em} = 660 nm). On the basis of

these data, we estimated the substituent effects for the red shift on the emission wavelength and rationally explained the results by DFT calculations. Furthermore, potential applicability of these fluorescent dyes to cell staining was exemplified.

Introduction

Xanthene-based fluorescent dyes represented by fluorescein (**1**) [1] have been widely used in the fields of molecular biology and medicinal chemistry.[2] Fluorescein and/or xanthene-based fluorescent dyes usually show emission at approximately 510 nm owing to the use of the xanthene skeleton as a common fluorophore. [3] To avoid overlap with the auto fluorescence of living organisms such as tryptophan and heme, many attempts have been reported to shift the emission wavelength of fluorescent dyes into the red or near infrared regions. In particular, the conversion of the oxygen at the 10-position of xanthenes to silicon [4] or phosphorus [5] has been shown to be effective for these purposes and widely investigated.

We have also been studying fluorescent dyes that show emission in the red/near infrared region based on xanthene frameworks by alternative approaches (Figure 1). First, we synthesized dinaphthofluorescein **2**, which features an expanded π-conjugate system, by the simple addition of benzene rings to both sides of fluorescein.[6] Compound **2** showed emission at 790 nm as expected; however, this molecule featured quite a low solubility in organic solvents and water with a low fluorescence quantum yield ($\Phi \leq 0.1\%$). On the basis of these results, we have tried to develop new fluorescent molecules that have a molecular weight comparable to that of fluorescein, but show absorption and emission at longer wavelengths than those of fluorescein. We recently developed V-shaped xanthene dyes **3** [7] and **4** [8], in which a xanthene skeleton and an aryl group are connected with an ether linkage, and the aryl group is incorporated into the π-system of the xanthene skeleton. The V-shaped **3** showed emission at wavelengths of 550 nm, reflecting a 40 nm red shift compared with that of fluorescein.

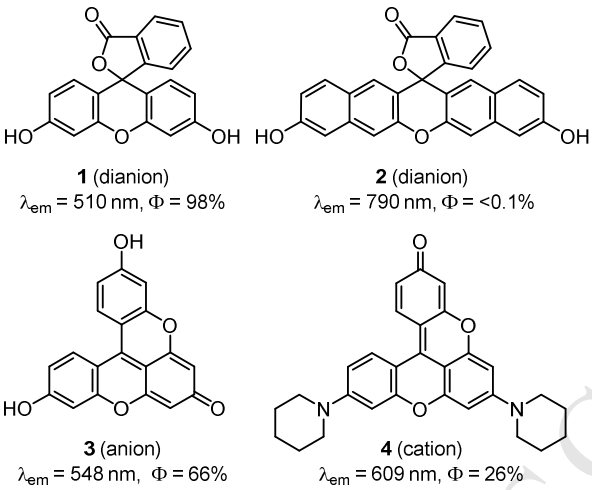

Figure 1. Structures of fluorescent dyes **1–4.**

In this manuscript, we will demonstrate an alternative approach, which involves connecting the aryl group to the xanthene skeleton through a triple bond, to achieve large red shifts in both the absorption and emission wavelengths. Fluorescein and its derivatives generally consist of a xanthene skeleton and an aryl group at 9-position, which although orthogonal to xanthene system does subtly interact. However, the acetylene linkages between the two moieties are in the same plane and expansion of the π system might be expected. Although, four similar fluorescent dyes connecting aryl groups and (pseudo)xanthene skeletons with acetylene moieties have been reported in patents [9] and papers [10], only phenyl and mesityl groups were investigated as the aryl groups (Figure 2). We believe that more extensive research on different substituents effects on the aryl groups and the role of acetylene linker could be useful, together with computational studies. In this study, we synthesized a variety of acetylene bridged xanthene dyes and revealed their photophysical properties, including substituent effects on the aryl group and solvatochromism, for applications to imaging of living cells.

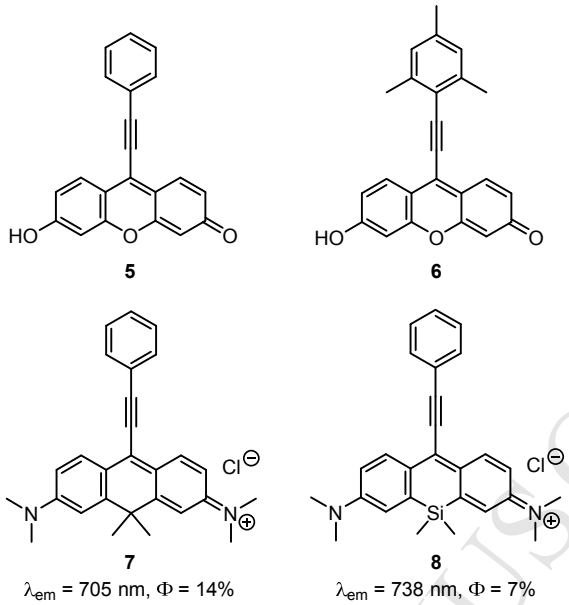

Figure 2. Four reported (pseudo)xanthene dyes with arylacetylene moieties.

Syntheses of acetylene bridged xanthene dyes 5 and 10–17

First, the acetylene bridged xanthene dyes **5** and **10–17** were synthesized according to a reported procedure (Scheme 1, method A).[9] Thus, the arylacetylenes were treated with *n*-BuLi to prepare corresponding lithium acetylides. These were then reacted with TBS protected xanthone **9** [11] to give intermediate **A**, followed by removal of the two TBS groups under HF-pyridine conditions to afford the desired acetylene bridged xanthene dyes **5**, **10**, and **11** [12] in yields of 67%, 83%, and 21%, respectively. However, in the case of a combination of lithium *p*-F-phenylacetylide and **9**, a trace amount of desired **12** was obtained, and deprotected xanthone **18** and TBS acetylene **19** were isolated in yields of 78% and 23%, respectively. Thus, the lithium acetylide predominantly attacked the silicon atoms of the protecting TBS group. These data indicate that the nucleophilicity of lithium acetylide possessing an electron withdrawing substituent on the aryl group was reduced, and its soft character was increased. To improve the selectivity and reactivity of lithium acetylide, anhydrous cerium chloride was added to the solution to generate the corresponding cerium acetylide in situ, according to Imamoto's procedure.[13] The cerium acetylide reacted smoothly with the carbonyl group on compound **9**, and the following deprotection of the two TBS groups of the phenolic hydroxy

groups was performed under acetic acid conditions to afford the desired acetylene bridged xanthenes **11–17** in moderate to high yields (Method B). Owing to the low yield of the 2-pyridiyl acetylene compound **15** (35%) obtained with the use of method B, a combination of LDA and $CeCl_3$ was used to obtain **15** in 65% yield (Method C). The yields of the products and the applied synthetic methods are summarized in Table 1.

Scheme 1. Synthesis of acetylene linked dyes **5** and **10**-**17**.

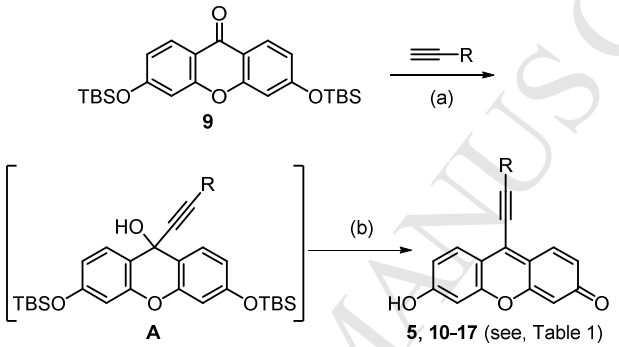

Method	(a)	(b)
A	*n*-BuLi	HF·pyridine
B	*n*-BuLi, $CeCl_3$	AcOH
C	LDA, $CeCl_3$	AcOH

Table 1. Yields and applied methods.

entry	product	R	Method	yield (%)
1	**5**	C_6H_5	A	67
2	**10**	*p*-OMe-C_6H_4	A	83
3	**11**	*p*-CF_3-C_6H_4	A	21
4			B	53
5	**12**	*p*-F-C_6H_4	A	trace[a]
6			B	60
7	**13**	*m*-F-C_6H_4	B	69
8	**14**	*o*-F-C_6H_4	B	68
9	**15**	2-pyridyl	B	35
10			C	65
11	**16**	TMS	B	58
12	**17**	Me	B	65

a) Compounds **18** and **19** were isolated as by-products.

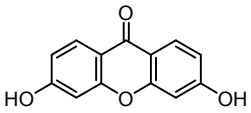

18 (78%)

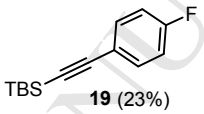

19 (23%)

Optical properties of the acetylene bridged xanthene dyes 5, and 10–17

With the nine xanthene dyes (**5**, and **10–17**) in hand, we investigated their optical properties. First, the simplest compound **5** was selected as a representative of the nine compounds, the pH response of compound **5** was investigated. Titration UV absorption spectra of compound **5** are shown in Figure 3a. The UV-vis spectrum of compound **5** showed sharp absorption at 608 nm under basic conditions (10 equiv. of tetrabutylammonium hydroxide) in DMSO. As acetic acid was added to the solution, the absorption at 608 nm gradually decreased and absorptions at 369 and 504 nm increased with isosbestic points at 386 and 536 nm.

These data suggested that compound **5** featured two forms (anionic and neutral forms) depending on the solution pH. The fluorescent quantum yields of compound **5** were measured under neutral (Φ = 4 %) and basic (Φ = 34 %) conditions. The sharp absorption of the UV-vis spectrum and high fluorescent quantum yield indicated that compound **5** showed higher performance under basic conditions. Therefore, the optical properties of other compounds **10–17** were examined under basic conditions.

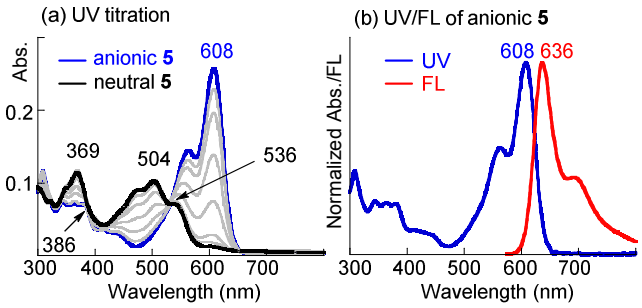

Figure 3. UV-vis titration of compound **5** with acid, and UV-vis absorption and FL spectra of anionic **5**: (a) UV-vis absorption spectra for conversion of neutral **5** to corresponding anionic material. (b) UV-vis absorption and fluorescence spectra of anionic **5**. Conditions: [**5**] = 1.0×10^{-5} M in DMSO at 25 °C.

Figure 3b shows the absorption and fluorescence spectra of the basic compound **5**. Measurements were performed in the presence of 10 equiv. of TBAOH in DMSO solution. The absorption and fluorescence spectra mirrored each other. The maximum emission wavelength (λ_{em}) was 636 nm and the fluorescence quantum yield (Φ) was 34%, with a Stokes shift of 28 nm. Spectral features of compounds **10–17** are shown in the Supplementary Material.

The optical properties (maximum absorption wavelength (λ_{abs}), molar absorption coefficient (ε), excitation wavelength (λ_{ex}), maximum emission wavelength (λ_{em}), fluorescence quantum yield (Φ), and the Stokes shift of the synthesized compounds **5**, and **10–17**, together with those of 6-hydroxy-9-methyl-3*H*-xanthene-3-one (**20**) [14,15] as a reference compound, are summarized in Table 2.

Table 2. Optical properties of compounds **5**, **10–17** and **20** (anionic form) in DMSO 25 °C.

Compound	λ_{abs} (nm)	ε ($\lambda_{abs.}$)	λ_{ex} (nm)	λ_{em} (nm)	Φ (%)[a]	Stokes shift (nm)
5 (*p*-H)	608	27,000	607	636	34	28
10 (*p*-OMe)	602	61,000	601	627	71	25
11 (*p*-CF_3)	622	40,000	620	660	24	38
12 (*p*-F)	607	60,000	607	636	55	29
13 (*m*-F)	614	45,000	615	647	34	33
14 (*o*-F)	615	53,000	615	646	38	31
15 (2-pyr)	620	38,000	620	656	32	36
16 (TMS)	602	72,000	602	623	52	21
17 (Me)	580	76,000	579	600	61	20
20	522	79,000	520	536	>98	14
11 (*p*-CF_3) [b]	552	36,000	552	595	5	43

[a] Based on a fluorescein in 0.1 M NaOH aq (Φ = 98%). [b] The UV-vis absorption and FL spectra were measured in 1 mM aqueous NaOH solution.

On the basis of the maximum emission wavelengths of the compounds in Table 2, the effects of substituents on increasing the emission wavelength were estimated. Thus, 6-hydroxy-9-methyl-3*H*-xanthene-3-one (**20**), which simply had a methyl group at the 9-position showed an emission wavelength at 536 nm, whereas compound **17**, possessing a methylacetylene group, showed emission at 600 nm. Therefore, the substituent effect of the acetylene bond was calculated to be approximately 64 nm. Furthermore, when methylacetylene of compound **17** was converted to phenylacetylene **5**, the emission wavelength shifted from 600 to 636 nm, such that the substituent effect of the phenyl group was estimated to be approximately 36 nm. Notably, the substituent effect of the acetylene bond was greater than that of the phenyl group on the xanthene derivatives.

Next, we considered the substituent effects on the terminal aromatic rings. In Figure 4a, the normalized fluorescent spectra of the selected compounds are shown. The λ_{em} of compound **5** (H at the *para* position), compound **10** (*p*-OMe), and compound **11** (*p*-CF_3) were 636, 627, and 660 nm, respectively. Thus, introducing an electron donating substituent caused a blue shift of the emission wavelength, and addition of an electron withdrawing substituent caused a red shift. Furthermore, in a

comparison of the regioisomeric compounds **12** (*p*-F), **13** (*m*-F), and **14** (*o*-F), the λ_{em} of compound **12** (*p*-F) was comparable to that of compound **5** (*p*-H). Therefore, introducing fluorine at the *para* position showed no substituent effect on the emission wavelength. The maximum emission wavelengths of **13** (*m*-F) and **14** (*o*-F) were at 647 and 646 nm, respectively. These data indicate that the fluorine at *meta* and *ortho* positions acted as an electron withdrawing substituent.

The relationship between the maximum emission wavelengths and Hammett's substituent constants (σ) [16, 17] is shown in Figure 4b. A quite high correlation (R = 0.98) was observed between them, suggesting that it is possible to predict the emission wavelength of compounds by applying this relationship.

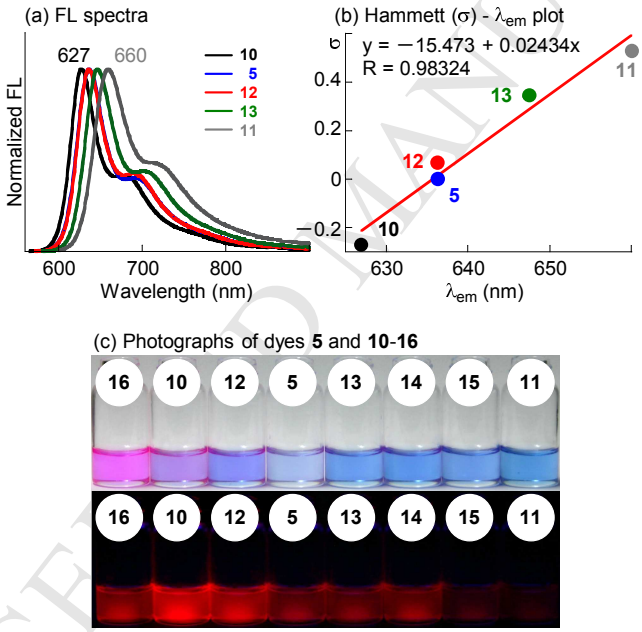

Figure 4. (a) Normalized fluorescent spectra of compounds **5** and **10–13**. (b) Relationship between the maximum emission wavelengths and Hammett's substituent constants. (c) Photographs of dyes (1.0×10^{-5} M in DMSO) obtained under white light (top) and 365 nm light (bottom).

Pictures of compounds **5**, and **10–16** under white light and black light (365 nm) are also shown in Figure 4c. Pink to blue coloration were observed under white light, and red emission was found under 365 nm irradiation.

Next, we investigated the solvatochromism of compound **11** (*p*-CF_3), which showed the longest emission wavelength among the nine compounds. The normalized FL spectra of compound

11 in various solvents under basic conditions are depicted in Figure 5a. The λ_{em} in FL spectra were shifted to longer wavelength in the order: MeOH, chloroform, acetonitrile, acetone, DMSO, and THF. A quite high correlation (R = 0.97) was confirmed between the maximum emission wavelength of compound **11** in various solvents and the acceptor number (Figure 5b). [18] The acceptor number (AN) is one solvent parameter that indicates the electron acceptability of the solvent. Thus, the solvatochromism of compound **11** can be explained by solvation. In MeOH, which has a high AN, the anionic compound **11** in the ground state was solvated by hydrogen bonding and the HOMO was stabilized. Therefore, the HOMO-LUMO gap increased and the UV-vis absorption and FL spectra were shifted to shorter wavelengths. Conversely, in non-protic and low AN solvents, such as acetonitrile, acetone, DMSO, and THF, the stabilization of anionic species of compound **11** in the ground state was low. Thus, negligible shifts were observed in the UV-vis and FL spectra. Photographs of the solutions under white light and 365 nm irradiation are shown in Figure 5c. The color of the solution under white light changed from magenta to blue, and red emission was detected for all solutions under 365 nm irradiation. The optical properties of compound **11** in various solvents are summarized in Table 3. The solvatochromism regarding the maximum emission wavelength ranged from 610 nm (MeOH) to 672 nm (THF), quantum yields were approximately 13–24%, and the Stokes shift was in the range of 38–44 nm.

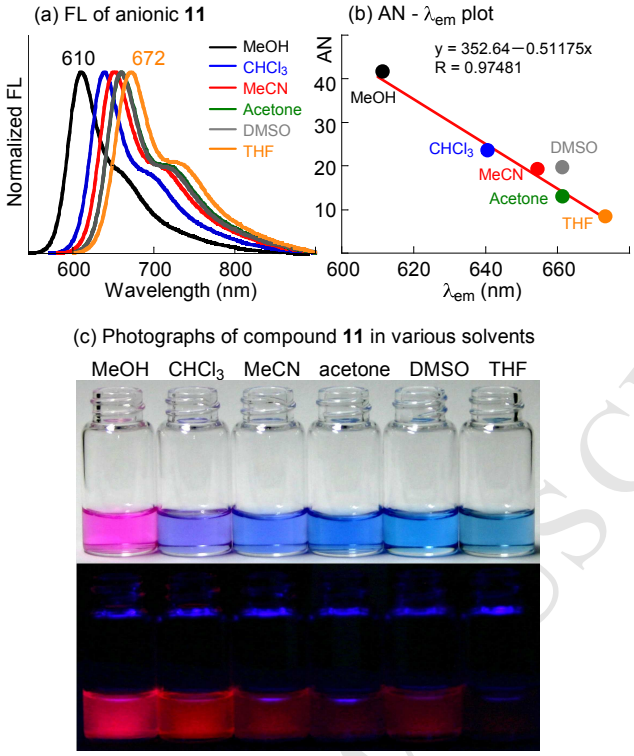

Figure 5. (a) Normalized emission spectra of compound **11** in various solvents, (b) relationship between λ_{em} and acceptor number (AN), (c) photographs of compound **11** (1.0×10^{-5} M in various solvents) obtained under white light (top) and 365 nm light (bottom).

Table 3. Optical properties of anionic compound **11** in various solvents at 25 °C.

Solvent	λ_{abs} (nm)	λ_{ex} (nm)	λ_{em} (nm)	Φ (%)[a]	Stokes shift (nm)
MeOH	571	570	610	22	39
$CHCl_3$	598	599	639	24	41
MeCN	610	612	653	19	43
Acetone	621	619	660	17	39
DMSO	622	620	660	24	38
THF	607/628	629	672	13	44

[a] Based on a fluorescein in 0.1 M NaOH aq (Φ = 98%).

Computational studies of the xanthene dyes [19]

DFT calculations at the B3LYP/6-31+G(d,p) level of theory indicated that the most stable conformation of compound **5** featured a perfect planner structure between the xanthene skeleton and the aryl group owing to no steric repulsion between the two moieties apart from the acetylene linker (Figure 6). The dihedral angle composed of four carbons (showed in blue in figure 6) was estimated to be 0.0°. Therefore, orbital interactions were expected between the xanthene skeleton and the aryl group through the acetylene linkage.

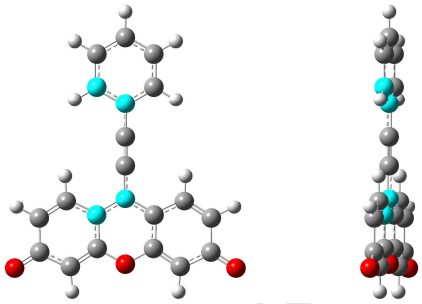

Figure 6. Most stable conformation of compound **5** obtained by DFT calculations at the B3LYP/6-31+G(d,p) level.; Front view (left) and side view (right).

Figure 7 shows the HOMOs, LUMOs, and energy gaps for the anionic forms of **20**, **17**, **10**, **5**, and **11**, respectively, with the observed and calculated absorption wavelengths.

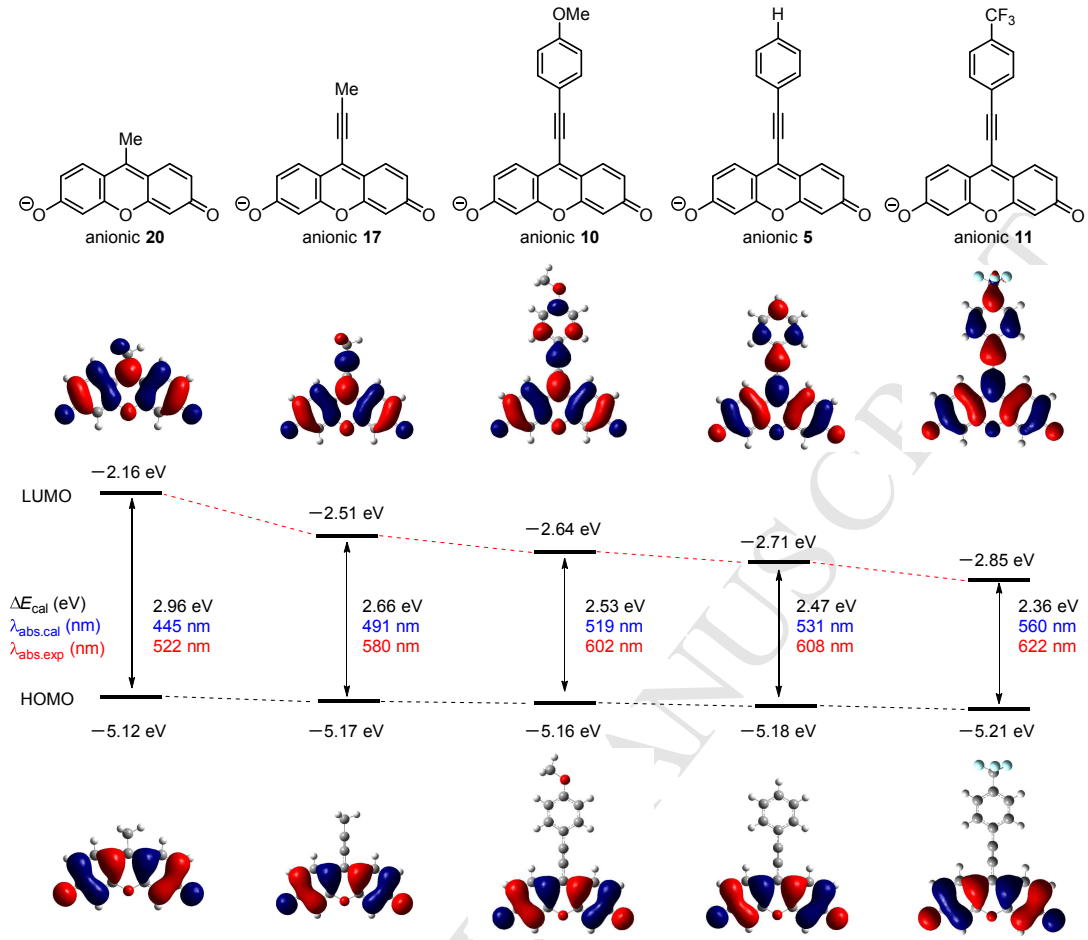

Figure 7. Energy diagrams and HOMOs-LUMOs for the anionic **20**, **17**, **10**, **5** and **11** in DMSO obtained by DFT calculations at the B3LYP/6-31+G(d,p) level and observed and estimated λ_{abs}.

Results of all calculations show that the HOMO is located on the xanthene skeleton, and the LUMO is spread over the whole molecule. Therefore, the arylacetylene moiety and/or substituents on the aryl group exert a greater influence on the level of LUMO than that of the HOMO. Comparing compound **20** with compound **17**, the LUMO is stabilized by approximately 0.35 eV through the addition of the acetylene moiety. A comparison of compounds **17** and **5** indicates that the LUMO is stabilized by approximately 0.20 eV through the incorporation of a benzene ring. Moreover, we examined the substituent effects of the aryl group, compounds **10**, **5**, and **11**. On the basis of the LUMO level of compound **5**, we found that the OMe group on the *para* position of compound **10** contributes to an increase of the LUMO level, conversely, the CF_3 group of compound **11** decreases the LUMO level. Therefore, the HOMO-LUMO gap increases in the compound **10** and decreases in compound **11**.

Next, we discuss the role acetylene and arylacetylene moieties in extending the π conjugation system. The measured absorption wavelength of compound **20** was 522 nm and that of compound **17** was 580 nm. Therefore, one acetylene moiety exerted a 58 nm shift of the absorption wavelength through π expansion. The calculated wavelengths for compounds **20** and **17** were 445 and 491 nm, respectively. The change in wavelength by the addition of an acetylene moiety was estimated to be 46 nm. Thus, the effect on π-extension by one acetylene moiety estimated by DFT calculation agreed well with the actual measurement. The role of the aryl group on π-extension is considered. The measured absorption wavelength of compound **17** was 580 nm and that of compound **5** was 608 nm. The degree of the wavelength shift exerted by one benzene ring is 28 nm. The calculated wavelengths of compounds **17** and **5** were 491 nm and 531 nm, respectively. Therefore, the change of the wavelength owing to the addition of one benzene ring was calculated to be 40 nm, which also matches with the actual measurement results. Notably, the effect of one acetylene moiety on the wavelength was the same or greater than that of one benzene ring, in both the actual and calculated measurements.

Confocal laser scanning microscopic observation of cells treated with compounds 10 and 11

Finally, cell staining experiments were performed for with a view to potential applications in bioimaging. Compound **10** (*p*-OMe), which had the highest quantum yield among the nine compounds, and compound **11** (*p*-CF_3), which emitted the longest wavelength, were chosen and applied for bioimaging. HeLa cells were incubated with compounds **10** and **11** (10 μM) in phosphate buffered saline (PBS) for 15 min, and then fluorescence signals in living cells were analyzed by confocal laser scanning microscopy (excitation 559 nm; emission 570-670 nm), respectively. The differential interference contrast (DIC), fluorescence and merged images are shown in Figure 8. It looks likely that both compounds stained cell membranes and membrane compartments in the cells. Of course further studies are needed, these results suggested the possibility of use of these compounds for cell staining.

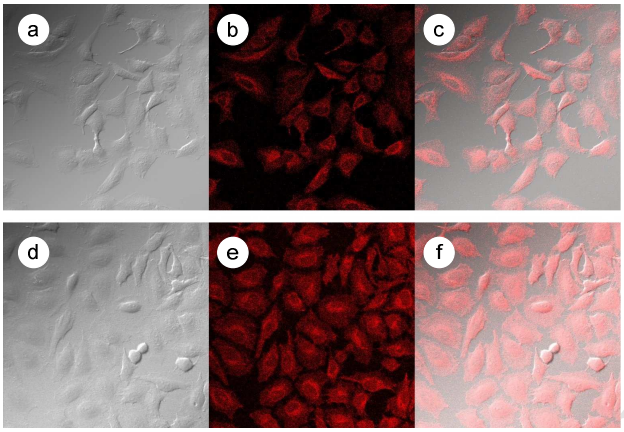

Figure 8. (a) DIC image of HeLa cells treated with compound **10**, (b) fluorescence image of compound **10** with 559 nm, (c) merged image of (a) and (b). (d) DIC image of HeLa cells treated with compound **11**, (e) fluorescence image of compound **11** with 559 nm, (f) merged images of (d) and (e).

Conclusion

We report the syntheses of xanthene fluorescent dyes possessing arylacetylenes and examine their properties and relationships among their structural features and red shifts of their emission wavelengths. For the synthesis, we proposed an improvement to the reactivity of the acetylide toward the carbonyl group of xanthone with the use of hard ceric chloride. Synthetic compounds having arylacetylenes showed emission wavelengths greater than 600 nm under basic conditions in DMSO. We found that the absorption and emission wavelength were blue shifted by the introduction of an electron donating substituent on the aryl group, and shifted in a red direction by the addition of an electron withdrawing substituent. These behaviors were clarified by DFT calculations, which showed that the substituent groups mainly affected the LUMO level. Potential applicability of the xanthene fluorescent dyes to cell staining was exemplified using compounds **10** and **11**. These compounds could be adjusted to more suitable and desirable emission regions for fluorescence microscopy measurements through the use of different substituents on the aryl groups.

Experimental

General procedure for the preparation of compounds **5** and **10–17**.

Method A. A solution of *n*-BuLi (1.64 M *n*-hexane solution; 2.38 mL, 3.9 mmol) was added dropwise to a solution of ethynylbenzene (0.51 mL, 4.6 mmol) in dry toluene (4 mL) under N_2 atmosphere at −78 °C. The reaction mixture was stirred for 30 min at 0 °C, and a solution of 3,6-bis(*tert*-butyldimethylsilyloxy)-9*H*-xanthene-9-one (**9**, 600 mg, 1.31 mmol) in dry toluene (8 mL) was subsequently added dropwise. The reaction mixture was stirred for 4 h at room temperature, and evaporated to dryness under a reduced pressure. The residue was dissolved in THF (7 mL), and a solution of HF-pyridine (13 M THF solution; 0.5 mL, 6.6 mmol) was added. The reaction mixture was stirred for 1.5 h at room temperature, and evaporated to dryness under a reduced pressure. The residue was washed with water and methanol, and the undissolved solid was collected by filtration to afford compound **5** (274 mg, 67% yield) as a dark red solid.

Compound **5** : 67% yield from compound **9** and ethynylbenzene. Dark red solid. Mp >300 °C. IR (KBr) 3060, 3043, 2200, 1828, 1795, 1747, 1698, 1635, 1590, 1506, 1457, 1417, 1380, 1315, 1270, 1205, 1178, 1103 cm^{-1}. ^1H NMR (400 MHz, DMSO-d_6) δ 8.00 (d, *J* = 8.8 Hz, 2H), 7.92 (m, 2H), 7.58 (m, 3H), 6.95–6.65 (br, 2H), 6.64–6.19 (br, 2H). ^{13}C NMR (100 MHz, DMSO-d_6) δ 132.6, 131.0, 130.1, 129.0, 128.8, 120.4, 107.8, 103.3, 82.1 (4 signals were not identified in spite of 13,824 number of scans). HRMS (FT-ICR-MS) calcd for $C_{21}H_{13}O_3$ $(M + H)^+$ 313.0859, Found 313.0859.

Compound **10** : 83% yield from compound **9** and 4-ethynylanisole. Red solid. Mp >300 °C. IR (KBr) 3465, 3432, 3396, 3060, 2919, 2848, 2593, 2559, 2186, 1633, 1598, 1511, 1490, 1467, 1428, 1380, 1340, 1299, 1259, 1209, 1172, 1105, 1041, 1016 cm^{-1}. ^1H NMR (400 MHz, DMSO-d_6) δ 7.97 (d, *J* = 9.2 Hz, 2H), 7.88 (d, *J* = 8.8 Hz, 2H), 7.11 (d, *J* = 8.8 Hz, 2H), 6.73 (d, *J* = 9.2 Hz, 2H), 6.52–6.37 (br, 2H), 3.87 (s, 3H). ^{13}C NMR (100 MHz, DMSO-d_6) δ 161.4, 134.7, 130.2, 129.5, 114.8, 112.2, 109.1, 103.2, 81.8, 55.5 (4 signals were not identified in spite of 24,576 number of scans). HRMS (FT-ICR-MS) calcd for $C_{22}H_{15}O_4$ $(M + H)^+$ 343.0965, Found 343.0968.

Compound **19** : 23% yield from compound **9** and 1-ethynyl-4-fluorobenzene. Yellow oil.

IR (neat) 3050, 2954, 2931, 2886, 2857, 2711, 2159, 2123, 1995, 1889, 1648, 1600, 1504, 1471, 1407, 1361, 1294, 1251, 1234, 1213, 1155, 1091, 1052, 1008. ^{1}H NMR (400 MHz, $CDCl_3$) δ 7.45 (dd, *J* = 8.8, 5.6 Hz, 2H), 6.99 (t, *J* = 8.8 Hz, 2H), 0.99 (s, 9H), 0.18 (s, 6H). ^{13}C NMR (100 MHz, $CDCl_3$) δ 162.6 (d, *J* = 248 Hz), 133.9 (d, *J* = 8.0 Hz), 119.4 (d, *J* = 4.0 Hz), 115.4 (d, *J* = 22.0 Hz), 104.6, 92.1 (d, *J* = 1.0 Hz), 26.1, 16.7, −4.6. HRMS (FT-ICR-MS) calcd for $C_{14}H_{20}FSi$ $(M + H)^+$ 235.1313, Found 235.1315.

Method B. A solution of *n*-BuLi (1.55 M *n*-hexane solution; 0.60 mL, 0.93 mmol) was added dropwise to a solution of 1-ethynyl-4-(trifluoromethyl)benzene (0.16 mL, 1.1 mmol) in dry THF (4 mL) under N_2 atmosphere at 0 °C. After stirring for 30 min at 0 °C, this solution was added to a suspension of cerium (III) chloride (247 mg, 1.0 mmol) in dry THF (2 mL) at −78 °C, and the whole mixture was stirred for further 30 min at −78 °C. A solution of 3,6-bis(*tert*-butyldimethylsilyloxy)-9*H*-xanthene-9-one (**9**, 140 mg, 0.31 mmol) in dry THF (2 mL) was subsequently added dropwise, and the reaction mixture was stirred for 1.5 h at 0 °C. The reaction mixture was quenched by sat. NH_4Cl aq. solution (5 mL), diluted with ethyl acetate (5 mL), and filtered through celite. The filtrate was extracted with ethyl acetate. The organic layer was washed sequentially with sat. NH_4Cl aq. solution, water (three times) and brine, and evaporated to dryness under a reduced pressure. The residue was dissolved in THF (2 mL) and water (2 mL), and acetic acid (2 mL) was added. After stirring for 10 min at room temperature, the undissolved solid was collected by filtration, and washed with water, chloroform, and methanol to afford compound **11** (63.0 mg, 53% yield) as a red solid.

Compound **11** : 53% yield from compound **9** and 1-ethynyl-4-(trifluoromethyl)benzene. Red solid. Mp 274–276 °C (decomp.). IR (KBr) 3064, 2925, 2757, 2597, 2202, 1635, 1616, 1563, 1492, 1465, 1428, 1380, 1322, 1276, 1209, 1174, 1105, 1068, 1016 cm^{-1}. ^{1}H NMR (400 MHz, DMSO-d_6) δ 8.15 (d, *J* = 8.0 Hz, 2H), 8.03 (d, *J* = 9.2 Hz, 2H), 7.92 (d, *J* = 8.0 Hz, 2H), 6.87–6.67 (br, 2H), 6.66–6.28 (br, 2H). ^{13}C NMR (100 MHz, DMSO-d_6) δ 133.4, 130.5, 130.2, 128.1, 127.4, 125.8, 125.7, 124.6, 105.3 (some signals were not identified in spite of 14,848 number of scans).

HRMS (FT-ICR-MS) calcd for $C_{22}H_{10}F_3O_3$ $(M - H)^-$ 379.0588, Found 379.0586.

Compound **12** : 60% yield from compound **9** and 1-ethynyl-4-fluorobenzene. Red brown solid. Mp >300 °C. IR (KBr) 3064, 2923, 2595, 2568, 2198, 1889, 1828, 1795, 1747, 1735, 1635, 1614, 1596, 1508, 1490, 1461, 1428, 1378, 1338, 1276, 1228, 1209, 1155, 1126, 1105, 1039 cm^{-1}. ^1H NMR (400 MHz, DMSO-d_6) δ 8.02 (dd, *J* = 8.8, 5.2 Hz, 2H), 8.00 (d, *J* = 9.2 Hz, 2H), 7.42 (t, *J* = 8.8 Hz, 2H), 6.82–6.64 (br, 2H), 6.59–6.32 (br, 2H). ^{13}C NMR (100 MHz, DMSO-d_6) δ 135.4 (d, *J* = 9.0 Hz), 130.2, 128.7, 116.4 (d, *J* = 23.0 Hz) (9 signals were not identified in spite of 18,227 number of scans). HRMS (FT-ICR-MS) calcd for $C_{21}H_{12}FO_3$ $(M + H)^+$ 331.0765, Found 331.0767.

Compound **13** : 69% yield from compound **9** and 1-ethynyl-3-fluorobenzene. Dark red solid. Mp >300 °C. IR (KBr) 3432, 3396, 3064, 2767, 2474, 2200, 1735, 1637, 1598, 1579, 1509, 1455, 1415, 1382, 1313, 1267, 1201, 1155, 1108, 1043, 1000 cm^{-1}. ^1H NMR (400 MHz, DMSO-d_6) δ 8.02 (d, *J* = 9.2 Hz, 2H), 7.89 (d, *J* = 8.8 Hz, 1H), 7.78 (d, *J* = 7.6 Hz, 1H), 7.60 (m, 1H), 7.46 (dt, *J* = 8.8, 2.0 Hz, 1H), 6.96–6.63 (br, 2H), 6.62–6.11 (br, 2H). ^{13}C NMR (100 MHz, DMSO-d_6) δ 131.2 (d, *J* = 8.0 Hz), 129.1 (d, *J* = 3.0 Hz), 128.4, 119.3 (d, *J* = 23.0 Hz), 118.3 (d, *J* = 21.0 Hz), 82.6 (9 signals were not identified in spite of 19,456 number of scans). HRMS (FT-ICR-MS) calcd for $C_{21}H_{12}FO_3$ $(M + H)^+$ 331.0765, Found 331.0767.

Compound **14** : 68% yield from compound **9** and 1-ethynyl-2-fluorobenzene. Purple solid. Mp 280–281 °C (decomp.). IR (KBr) 3058, 3039, 2474, 2204, 1828, 1795, 1749, 1700, 1635, 1589, 1536, 1502, 1457, 1419, 1380, 1336, 1272, 1209, 1176, 1103 cm^{-1}. ^1H NMR (400 MHz, DMSO-d_6) δ 8.00 (t, *J* = 8.0 Hz, 1H), 7.89 (d, *J* = 9.2 Hz, 2H), 7.66 (m, 1H), 7.48 (t, *J* = 8.8 Hz, 1H), 7.40 (t, *J* = 8.0 Hz, 1H), 6.82–6.59 (br, 2H), 6.58–6.19 (br, 2H). ^{13}C NMR (100 MHz, DMSO-d_6) No meaningful signal was observed in spite of 21,504 number of scans. HRMS (FT-ICR-MS) calcd for $C_{21}H_{12}FO_3$ $(M + H)^+$ 331.0765, Found 331.0767.

Compound **16** : 58% yield from compound **9** and trimethylsilylacetylene. Red brown solid. Mp 243–244 °C (decomp.). IR (KBr) 2958, 2896, 2767, 2584, 2460, 1828, 1747, 1683, 1635, 1563, 1517, 1455, 1417, 1380, 1324, 1270, 1249, 1197, 1159, 1108, 1063 cm^{-1}. ^1H NMR (400 MHz, DMSO-d_6) δ 7.74 (d, *J* = 9.2 Hz, 2H), 6.73 (d, *J* = 9.2 Hz, 2H), 6.54–6.29 (br, 2H), 0.37 (s, 9H). ^{13}C

NMR (100 MHz, DMSO-d_6) δ 129.8, 128.1, 115.7, 103.3, 96.2, −0.56 (4 signals were not identified). HRMS (FT-ICR-MS) calcd for $C_{18}H_{16}O_3SiNa$ $(M + Na)^+$ 331.0761, Found 331.0769.

Compound **17** : 65% yield from compound **9** and propyne. Red solid. Mp 176–177 °C (decomp.). IR (KBr) 2503, 2219, 1828, 1747, 1698, 1635, 1585, 1544, 1504, 1457, 1417, 1380, 1334, 1268, 1207, 1159, 1095. ^{1}H NMR (400 MHz, DMSO-d_6) δ 11.4–10.8 (br, 1H), 7.82 (d, *J* = 9.2 Hz, 2H), 7.18–5.61 (br, 4H), 2.39 (s, 3H). ^{13}C NMR (100 MHz, DMSO-d_6) δ 130.1, 108.5, 72.7, 5.07 (6 signals were not identified in spite of 13,312 number of scans). HRMS (FT-ICR-MS) calcd for $C_{16}H_{11}O_3$ $(M + H)^+$ 251.0703, Found 251.0703.

Method C. Compound **15** : A solution of *n*-BuLi (1.55 M *n*-hexane solution; 0.60 mL, 0.93 mmol) was added dropwise to a solution of diisopropylamine (0.22 mL, 1.6 mmol) in dry THF (2 mL) under N_2 atmosphere at 0 °C, and the reaction mixture was stirred for 20 min at 0 °C. 2-Ethynylpyridine (0.11 mL, 1.1 mmol) was then added dropwise, and the reaction mixture was stirred for an additional 30 min at 0 °C. This solution was added to a suspension of cerium (III) chloride (247 mg, 1.0 mmol) in dry THF (2 mL) at −78 °C, and the whole mixture was stirred for further 30 min at −78 °C. A solution of 3,6-bis(*tert*-butyldimethylsilyloxy)-9*H*-xanthene-9-one (**9**, 140 mg, 0.31 mmol) in dry THF (2 mL) was subsequently added dropwise, and the reaction mixture was stirred for 1.5 h at 0 °C. The reaction mixture was quenched by sat. NH_4Cl aq. solution (5 mL), diluted with ethyl acetate (5 mL), and filtered through celite. The filtrate was extracted with ethyl acetate. The organic layer was washed sequentially with sat. NH_4Cl aq. solution, water (three times) and brine, and evaporated to dryness under a reduced pressure. The residue was dissolved in THF (2 mL) and water (2 mL), and acetic acid (2 mL) was added. After stirring for 10 min at room temperature, the undissolved solid was collected by filtration, and washed with water and chloroform to afford compound **15** (62.7 mg, 65% yield) as a purple solid. Mp 185–186 °C (decomp.). IR (KBr) 3432, 3394, 3052, 2483, 2208, 1828, 1795, 1747, 1639, 1585, 1558, 1504, 1459, 1436, 1419, 1382, 1334, 1315, 1268, 1207, 1176, 1101 cm^{-1}. ^{1}H NMR (400 MHz, DMSO-d_6) δ 8.75 (dt, *J* = 4.8, 1.6 Hz, 1H), 8.06 (dt, *J* = 7.6, 1.2 Hz, 1H), 8.00 (td, *J* = 7.6, 1.6 Hz, 1H), 7.94 (d, *J* = 9.2

Hz, 2H), 7.58 (ddd, *J* = 7.6, 4.8, 1.2 Hz, 1H), 6.77 (d, *J* = 9.2 Hz, 2H), 6.61–6.36 (br, 2H). ^{13}C NMR (100 MHz, DMSO-d_6) δ 150.7, 137.2, 128.9, 127.8, 125.2 (9 signals were not identified in spite of 13,312 number of scans). HRMS (FT-ICR-MS) calcd for $C_{20}H_{12}NO_3$ $(M + H)^+$ 314.0812, Found 314.0812.

Treatment of cells with compounds **10** and **11**.

HeLa cells (2×10^5 cells/dish) were seeded in 35 mm (φ) glass based dishes (Iwaki) in α-minimum essential medium supplemented with 10% (v/v) heat-inactivated bovine serum, and cultured for 24 h (80−90% confluence) at 37°C in a humidified incubator supplied with 5% CO_2 gas.

The medium was removed and the cells were washed twice with PBS(+) (137 mM NaCl, 8.1 mM Na_2HPO_4, 2.68 mM KCl, 1.47 mM KH_2PO_4, 0.33 mM $MgCl_2$, and 0.90 mM $CaCl_2$, pH 7.4) and treated with compounds **10** and **11** (final concentration 10 μM) in PBS(+) for 15 min at room temperature, respectively. The intracellular distribution of the each compound was analyzed without fixing the cells using a confocal scanning laser system (FV1000, Olympus) consisting of an inverted microscope (IX81, Olympus) equipped with a 40× UPlanSApo objective (dry, NA 0.95) (Ex. 559 nm; Em. 570–670 nm).

Acknowledgment

This study was supported in part by KAKENHI (Nos. 26293005 and 15K14931). This study was carried out using the Fourier transform ion cyclotron resonance mass spectrometer in the Joint Usage/Research Center at the Institute for Chemical Research, Kyoto University.

References and notes

(1) Baeyer, A. *Ber. Dtsch. Chem. Ges.* **1871**, *4*, 555–558.

(2) (a) de Silva, A. P.; Gunaratne, H. Q. N.; Gunnlaugsson, T.; Huxley, A. J. M.; McCoy, C. P.; Rademacher, J. T.; Rice, T. E. *Chem. Rev.* **1997**, *97*, 1515–1566. (b) Kobayashi, H.; Ogawa, M.; Alford, R.; Choyke, P. L.; Urano, Y. *Chem. Rev.* **2010**, *110*, 2620–2640. (c) Kikuchi, K. *Chem. Soc.*

Rev. **2010**, *39*, 2048–2053. (d) Lavis, L. D.; Raines, R. T. *ACS Chem*. *Biol*. **2014**, *9*, 855–866. (e) Niu, L. Y.; Chen, Y. Z.; Zheng, H. R.; Wu, L. Z.; Tung, C. H.; Yang, Q. Z. *Chem*. *Soc*. *Rev*. **2015**, *44*, 6143–6160. (f) Chen, X.; Wang, F.; Hyun, J. Y.; Wei, T.; Qiang, J.; Ren, X.; Shin, I.; Yoon, J. *Chem*. *Soc*. *Rev*. **2016**, *45*, 2976–3016. (g) Wu, D.; Sedgwick, A. C.; Gunnlaugsson, T.; Akkaya, E. U.; Yoon, J.; James, T. D. *Chem*. *Soc*. *Rev*. **2017**, *46*, 7105–7123.

(3) Urano, Y.; Kamiya, M.; Kanda, K.; Ueno, T.; Hirose, K.; Nagano, T. *J*. *Am*. *Chem*. *Soc*. **2005**, *127*, 4888–4894.

(4) For fluorescein types; (a) Egawa, T.; Koide, Y.; Hanaoka, K.; Komatsu, T.; Terai, T.; Nagano, T. *Chem*. *Commun*. **2011**, *47*, 4162–4164. (b) Best, Q. A.; Sattenapally N.; Dyer, D. J.; Scott, C. N.; MaCarroll, M. E. *J. Am. Chem. Soc*. **2013**, *135*, 13365–13370. (c) Hirabayashi,K.; Hanaoka, K. Takayanagi, T. Toki, Y.; Takahiro Egawa, T.; Kamiya, M.; Komatsu, T.; Ueno, T.; Terai, T.; Yoshida, K.; Uchiyama, M.; Nagano, T.; Urano Y. *Anal. Chem*. **2015**, *87*, 9061–9069. For rhodamine- and rhodol-types; (d) Zhou, P.; Ning, C.; Alasedi, A.; Han, K. *ChemPhysChem*. **2016**, *17*, 3139–3145. (e) Grimm, J. B.; Brown, T. A.; Tkachuk, A. N.; Lavis, L. D. *ACS Cent. Sci.* **2017**, *3*, 975–985. (f) Iwatate, R. J.: Kamiya, M.; Umezawa, K.; Kashima, H.; Kakadate, M.; Kojima, R.; Urano, Y. *Bioconjugate Chem*. **2018**, *29*, 241–244.

(5) (a) Fukazawa, A.; Suda, S.; Taki, M.; Yamaguchi, E.; Grzybowski, M.; Sato, Y.; Higashiyama, T.; Yamaguchi, S. *Chem*. *Commun*. **2016**, *52*, 1120–1123. (b) Fukazawa, A.; Usuba, J.; Adler, R. A.; Yamaguchi, S. *Chem*. *Commun*. **2017**, *53*, 8565–8568. (c) Ogasawara, H.; Grzybowski, M.; Hosokawa, R. Sato, Y.; Taki, M.; Yamaguchi, S. *Chem*. *Commun*. **2018**, *54*, 299–302.

(6) Azuma, E.; Nakamura, N.; Kuramochi, K.; Sasamori, T.; Tokitoh, N.; Sagami, I.; Tsubaki, K. *J*. *Org*. *Chem*. **2012**, *77*, 3492–3500.

(7) Yamagami, A.; Ishimura, H.; Katori, A.; Kuramochi, K.; Tsubaki, K. *Org*. *Biomol*. *Chem*. **2016**, *14*, 10963–10972.

(8) Yamagami, A.; Kawano, K.; Futaki, S.; Kuramochi, K.; Tsubaki, K. *Tetrahedron* **2017**, *73*, 7061–7066.

(9) Ustinov, A.; Korshun, V. US Pat. 2012/0316319 A1, 2012.

(10) (a) Pastierik, T.; Sebej, P.; Medalova, J.; Stacko, P.; Klan, P. *J. Org. Chem.* **2014**, *79*, 3374–3382. (b) Wei, L.; Chen, Z.; Shi, L.; Long, R.; Anzalone, A. V.; Zhang, L.; Hu, F.; Yuste, R.; Cornish, V. W.; Min W. *Nature*, **2017**, 544, 465–470.

(11) Shieh, P.; Hangauer, M. J.; Bertozzi, C. R. *J. Am. Chem. Soc.* **2012**, *134*, 17428−17431.

(12) On the basis of the bleaching curve of compound **11** measured by UV-vis, the half-life of decomposition was estimated to be 76.7 days. See Supplementary Material (Figure S2).

(13) Imamoto, T.; Sugiura, Y.; Takiyama, N. *Tetrahedron Lett.* **1984**, *25*, 4233–4236.

(14) (a) Sebej, P.; Wintner, J.; Muller, P.; Slanina, T.; Anshori, J. A.; Antony, L. A. P.; Klan, P.; Wirz, J. *J. Org. Chem.* **2013**, *78*, 1833–1843. (b) Martinez-Peragon, A.; Miguel, D.; Jurado, R.; Justicia, J.; Alvarez-Pez, J. M.; Cuerva, J. M.; Crovetto, L. *Chem. Eur. J.* **2014**, *20*, 447–455.

(15) Among these fluorescent dyes, the quantum yield of compound **20** is higher than those of **5** and **10**-**17**. This can be explained by the small thermal deactivation of the exited state due to its compact molecular shape.

(16) Hansch, C.; Leo, A.; Taft, R. W. *Chem. Rev.* **1991**, *91*, 165–195.

(17) Hammett, L. P. *J. Am. Chem. Soc.* **1937**, *59*, 96–103.

(18) Mayer, U.; Gutmann, V.; Gerger, W. *Monatsh. Chem.* **1975**, *106*, 1235–1257.

(19) Gaussian 09, Revision D.01, Frisch, M. J.; Trucks, G. W.; Schlegel, H. B.; Scuseria, G. E.; Robb, M. A.; Cheeseman, J. R.; Scalmani, G.; Barone, V.; Mennucci, B.; Petersson, G. A.; Nakatsuji, H.; Caricato, M.; Li, X.; Hratchian, H. P.; Izmaylov, A. F.; Bloino, J.; Zheng, G.; Sonnenberg, J. L.; Hada, M.; Ehara, M.; Toyota, K.; Fukuda, R.; Hasegawa, J.; Ishida, M.; Nakajima, T.; Honda, Y.; Kitao, O.; Nakai, H.; Vreven, T.; Montgomery, J. A.; Jr., Peralta, J. E.; Ogliaro, F.; Bearpark, M.; Heyd, J. J.; Brothers, E.; Kudin, K. N.; Staroverov, V. N.; Kobayashi, R.; Normand, J.; Raghavachari, K.; Rendell, A.; Burant, J. C.; Iyengar, S. S.; Tomasi, J.; Cossi, M.; Rega, N.; Millam, J. M.; Klene, M.; Knox, J. E.; Cross, J. B.; Bakken, V.; Adamo, C.; Jaramillo, J.; Gomperts, R.; Stratmann, R. E.; Yazyev, O.; Austin, A. J.; Cammi, R.; Pomelli, C.; Ochterski, J. W.; Martin, R. L.; Morokuma, K.; Zakrzewski, V. G.; Voth, G. A.; Salvador, P.; Dannenberg, J. J.; Dapprich, S.; Daniels, A. D.; Farkas, O.; Foresman, J. B.; Ortiz, J. V.; Cioslowski, J.; Fox, D. J. Gaussian, Inc., Wallingford CT, 2009.